STARS' CENTROID DETERMINATION USING PSF-FITTING METHOD

Robert Suszyński, Krzysztof Wawryn

Koszalin University of Technology, Faculty of Electronics and Information Technology, Śniadeckich 2, 75-543 Koszalin, Poland
(✉ roberts@tu.koszalin.pl, +48 94 347 8707, krzysztof.wawryn@tu.koszalin.pl)

Abstract

This paper presents an algorithm for restoring telescope images corrupted by turbulence effects and readout noise of a telescope system in order to determine centroid positions of stars, especially the position of a reference star. A computation method employing an accurate centroid estimation algorithm reconstructing a *point spread function* (PSF) from the recorded astronomical images has been used. Minimisation of turbulence effects and telescope control system noise in long exposure images acquired and recorded by the ground telescope is proposed. As a solution of the distortion error a minimisation signal is dedicated to GoTo calibration procedures built in control mechanisms of the electromechanical telescope system. The proposed method has been verified in the Matlab environment for real deep sky images recorded by the ground telescope system.

Keywords: centroid estimation, PSF-fitting, image processing.

1. Introduction

Astronomical images acquired by the ground telescopes are distorted by several sources. Atmospheric turbulence effects, readout noise and non-idealities in telescope mechanisms are the dominant sources of telescope image distortions. An *adaptive optics* (AO) system of the telescope is used to restore real images. The aim of the AO is to filter the distortions from the deep sky image and to generate a compensatory signal to control the telescope corrector [1–5]. Determination of the star position – called a centroid detection – is one of the main AO tasks. The position of a reference star is determined as the first task, and then positions of the other stars in the telescope image are determined in relation to the position of the reference star [6]. The centroid detection has to be preceded by filtering out the image distortions. Many different computation methods are adopted to reduce the image distortions [7–10]. Mathematically simplest methods are based on computing the centre of mass [11] and the weighted centre of mass [12–14] of a star, respectively. A Gaussian pattern matching [15] is also used in the centroid detection. Very popular centroid detection algorithms employ turbulence prediction methods adopting Zernike polynomials [16] and a principal component analysis with Kalman filtering [17]. Those methods are time-consuming, particularly if a polynomial degree is high. The turbulence prediction may be determined by a Bayesian estimation theory [18] as well.

The proposed method of stars' centroids detection in the *Deep Sky Object* (DSO) astronomical images is based on generation of an error minimisation signal to compensate turbulence effects and readout noise of the ground telescope system. In Section 2, the influence of the atmospheric turbulence and equipment noise on the quality of astronomical images is described. A computation method employing an accurate centroid estimation algorithm reconstructing a *point spread function* (PSF) from images is presented in Section 3. The method was introduced at ICSES'2014 [6]. This publication is an extension of the paper included in the conference proceedings. Additionally, it presents the detailed procedure performed in real

astronomical image processing. So far PSF was used for post-processing and enhancing the quality of already obtained astronomical images [19–22]. The novelty we propose in this paper is application of PSF during an observation session to improve the accuracy of reference star's centroid in real-time tracking systems during the long exposure sky object photography. In this work we additionally describe in detail the whole process of PSF reconstruction from the recorded astronomical images and its subsequent use in processing the successive recorded images. Processing of astronomical images using PSF is illustrated in Section 4. For verification purposes, the obtained results are compared with the results obtained by two standard methods.

2. Influence of atmospheric turbulence and equipment noise on centroid accuracy

During astronomical observation only a small amount of light reaches the telescope's CCD detector. Therefore, a long exposure to light is required to acquire and record such images. The same fragment of the sky has to be photographed by the telescope's CCD detector in the period of even several minutes. To satisfy that requirement, the ground telescope position should be changed to compensate the earth revolving movement. The required movement of the telescope depends on the geographic position of the telescope and the position of an observed sky object. Regardless of the appropriate correction of the telescope position, the distortions from different sources (such as turbulence effects, CCD detector noise and telescope mechanical vibrations) have to be filtered out from the astronomical images .
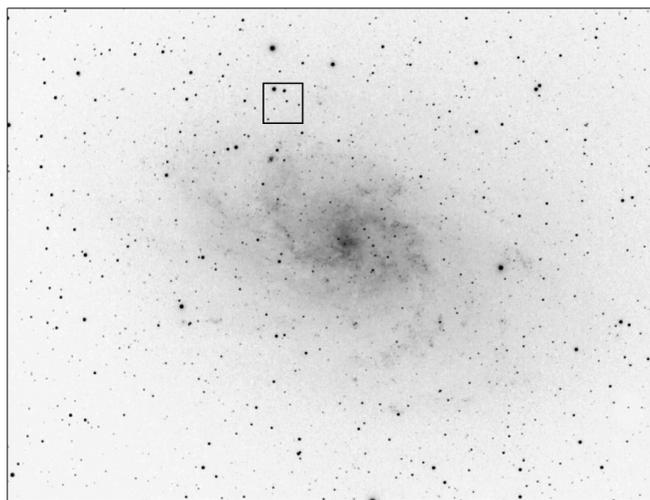

Fig. 1. A picture of M33 Galaxy, a group of stars is marked and chosen for the next calculation.
The picture: Robert Suszyński, refractor SW80ED 80/600mm, camera SBIG ST-2000XM,
stacking 13 images with exposure of 300 s each.

Atmospheric turbulence effects are the dominant sources of telescope image distortions. The distortions are caused by the following agents: differences in air density and temperature on different altitudes, movement of masses of atmosphere, and pollution by the cosmic dust and gases. The atmospheric sources of image distortions are also lights from the nearest neighbourhood such as street and advertisement lights, flare-up and reflection lights.

CCD detector noise follows the Poisson statistical distribution rule. The signal to noise ratio increases with the increase in the arrival rate of photons at the CCD detector. The dark fragments of the image are more noisy than the bright ones. To achieve better quality images, a long exposure time of the CCD detector has to be applied.

The telescope's mechanical vibrations are caused by telescope drives, gusts of wind, fast temperature changes and precipitations. A precise mounting of the drives-telescope-camera CCD system leads to significant reduction in the mechanical vibrations and their contribution to the astronomic image distortions.

Reduction of the atmospheric turbulence effects in the astronomic image distortions is a very difficult task. In this paper, a novel method to compensate for atmospheric turbulence effects in the AO system is proposed.

3. Determination of Point Spread Function by atmospheric turbulence and optic errors

Conditions of observations during one session are usually the same or very similar. The weather conditions, atmosphere turbulences and telescope system have stable parameters that directly influence the distortions of recorded astronomical images. They may be characterized by the PSF describing the degree of spreading (blurring) of the point object over a region on the CCD detector (a group of pixels – subdetection area) [19–22]. The PSF can be expressed by the following equation:

$$\mu(x, y) = \frac{1}{2\pi\delta} exp\left[-\frac{(x - X)^2 + (y - Y)^2}{2\delta^2} \right], \tag{1}$$

where: δ denotes the standard deviation, X and Y denote coordinates of the highest value centre point.

The PSF may be determined numerically from an analysis of the recorded images. It describes the image distortions as a result of atmospheric conditions and parameters of the recording equipment in a particular observation session, and may be used to perform subsequent images. This result enables using the PSF-fitting method to determine the positions of stars in the subsequent recorded images.

3.1. PSF calculation for a particular observation session

To improve determination of stars' centroids, using the PSF-fitting method [23, 24] is proposed. In a particular observation session, a test image is acquired in order to determine the PFS describing the present atmospheric conditions and optical equipment parameters. The test image is acquired several times, and the averaged PSF for several stars is calculated as a pattern function. Calculations of the averaged PSF are time-consuming, but performed only once – at the beginning of the observation session.

The appropriate choice of stars for PSF calculation is of a vital importance. They must be stars of relative brightness corresponding to 0.50–0.75 of the dynamic range of the CCD detector. For darker stars, PSF calculation will be subjected to large errors stemming from a high level of noise. For too bright stars, however, saturation will occur accompanied with an incorrect flattening of the PSF centre part. For a reference image that usually includes more than a dozen stars, this condition is easy to meet and the choice of stars can be made either automatically or with the assistance of the user.

4. Image processing using PSF-fitting method

4.1. Examined objects

The proposed method of centroid determination based on PSF-fitting has been tested on real images of astronomical objects. The necessary calculations have been performed on a series of 13 images of M33 Galaxy. The stacking results are shown in Fig. 1.

The images have been acquired with a monochromatic astronomy camera ST-2000XM and a SkyWatcher 80ED telescope with aperture: 80 mm and focal length: 600 mm, on an EQ6 SynScan equatorial mount. Every image has been acquired within the exposure time of 300 seconds. A series of images have been recorded during one night, in the same weather conditions, by the same telescope system.

4.2. PSF reconstructing for particular observation

At the beginning of the observation session, 20 test images of M33 Galaxy were taken, with the exposure time of 10 seconds. They were later used for calculating an averaged PSF. The short exposure time of images excludes errors resulting from inaccuracies of the telescope's drive, and yet it is sufficient to correctly record the star objects. Next, the proper observation session was started and a series of 15 images were taken, with a long exposure time of 300 seconds. 13 correct images were selected from this session for further calculations. This selected series of images were used for examining the accuracy of determining the star's centroid with the PSF-fitting method and comparing it with that of the standard method.

During the processing and analysis of the data from the first series of test images, a high quality image was selected, and a single bright star was chosen (with the brightness of 0.63 of the dynamic range of CCD sensor) near the rectangular area selected in Fig. 1. On the basis of this star's image, the PSF was calculated and next used in subsequent calculations.

The calculated averaged PSF shown in Fig. 2 can be used in processing subsequently recorded images. In order to simplify further calculations, the obtained function has been normalized in such a way that its values were contained within the full range of 8-bit numbers. The resolution of the averaged PSF is 10 x 10 times greater than the resolution of recorded images. It enables a 10 x10 times increase in the accuracy of stars' coordinates in the subsequent images. In order to determine the star position, the averaged PSF is correlated with the star image in an area of a few pixels within the expected position of the star. The obtained maximal image correlation value is used to determine the shifted position of the star. Calculations are not time-consuming and may be accomplished in real time for several stars. Application of greater resolution of the averaged PSF enables obtaining star centroid calculations with the 1/10 pixel accuracy and reduction of turbulence effects, CCD detector noise and telescope mechanical vibrations.
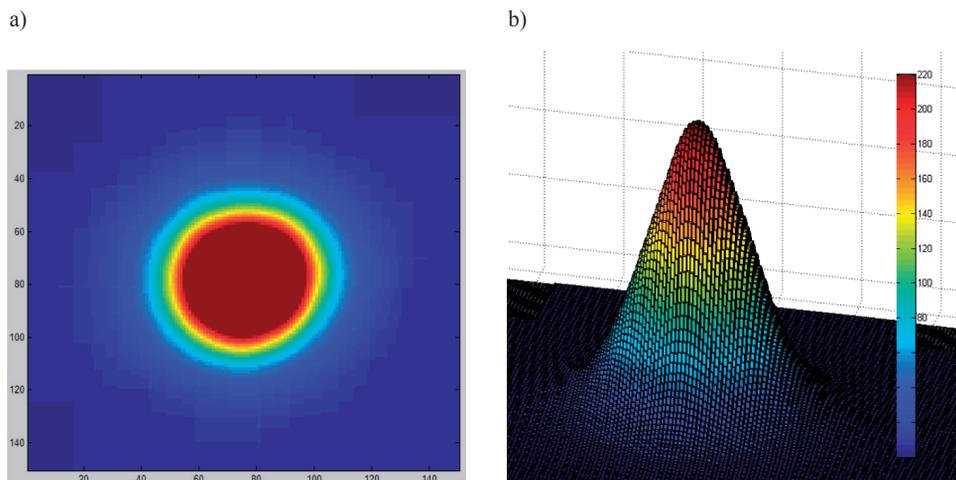
a)   b)

Fig. 2. The reconstructed PSF used for the subsequent calculation. Source: Own Matlab calculation.

4.3. Calculation of stars' centroids with PSF-fitting and two standard methods

To verify the proposed PSF-fitting method, extra calculations for two standard methods based on computing the star's centre of mass and the weighted centre of mass have been performed. Three stars denoted S1, S2 and S3, shown in Fig. 3, have been chosen for the next calculation. The stars have different relative brightness. The brightest S1 is recorded in the area of 15 x15 pixels. Its central part is bright, because its value exceeds the maximum value of 16 bit CCD and its light saturates the detector. The S2 is recorded in the whole range of CCD dynamics and its shape has sharp edges. The darkest S3 is recorded indistinctly, because 300 seconds is too short a time to obtain enough light for this star. It is obvious that stars S1 and S3 cannot be used as the reference ones. We performed calculations for them only to test the described methods in the case of too bright and too dim stars, and to consider the extreme cases. For ease of further calculations, the stars' images were normalized to 8-bit values.
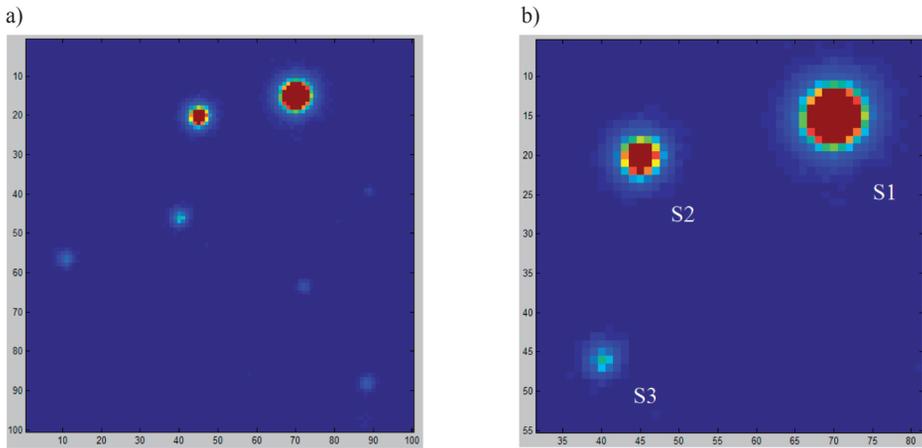

Fig. 3. a) A group of stars visible in a selected rectangular area of the whole photography from Fig. 1; b) stars S1, S2, S3 chosen for the next calculation. Source: Own Matlab calculation.

The S1 star in the selected images in a series of 13 photographs of M33 Galaxy is shown in Fig. 4. These images were used in further calculations. Comparison of them clearly shows the shift of the star, but also changes of its shape and brightness. These distortions greatly complicate correct determination of the star's centroid and calculating the shift of the subsequent recorded images.
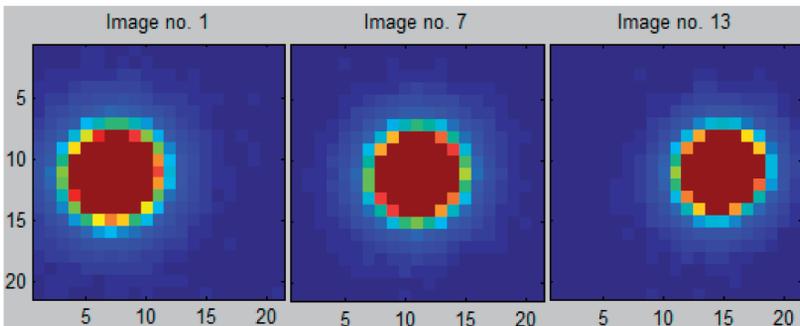

Fig. 4. The reference star S1 in the selected images in a series of 13 photographs of M33 Galaxy. Source: Own Matlab calculation.

To create reference data for the three tested methods, a calibration procedure of a series of thirteen M33 Galaxy images has been performed. Flat, dark and biased pictures [1] have also been taken into consideration. During the calibration process, a correlation of images, using 126 stars, has been done. The proposed method is reliable, but requires complicated calculations and cannot be done in real-time systems. After calibration, we obtain data about movement between images from the series.

The star brightness threshold cut-off is taken into consideration in the method based on calculating the star's centre of mass. In the second method, using the weighted centre of mass of a star, such a cut-off in not necessary. The weight represents brightness of each pixel inside the star contour. To determine the star's centroid, both methods are using calculation of the centre of mass of a plane figure. An example of the S2 star contour is presented in Fig. 5.
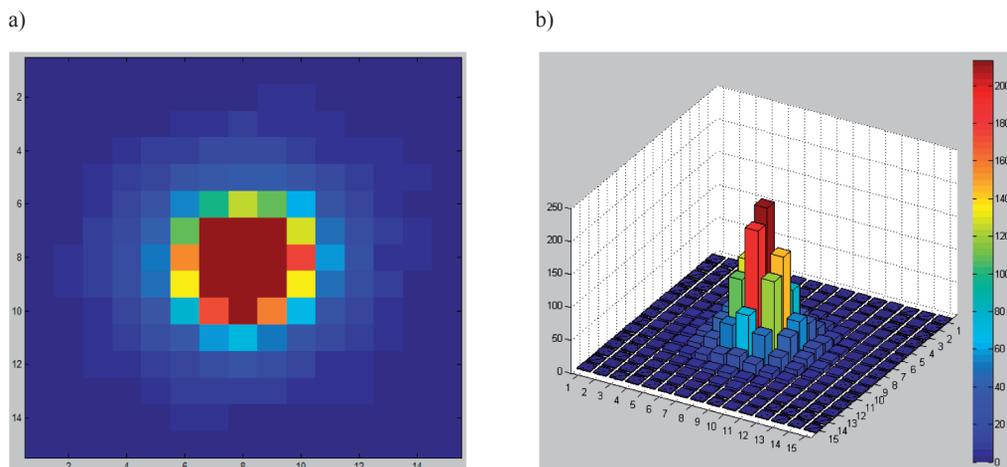
a)

b)

Fig. 5. a) The S2 star; b) an example of contour of a bright star. Source: Own Matlab calculation.

Suitable calculations of the above mentioned methods have been performed for a series of thirteen images of M33 Galaxy and the obtained results are presented in Table 1. For simplification, only the position shift in coordinate *x* is presented. The relative shifts are calculated in relation to the image number 7.

The results of the accuracy of centroid determination obtained by the proposed method and two standard methods for reference, for a series of thirteen real images of M33 Galaxy are presented in Table 1.

The calculated results for the two standard methods, the proposed PSF-fitting method and the reference data are presented in Tab. 1. The first standard method – the centre of mass method – is illustrated in Fig. 6. The presented results exhibit a small accuracy and large errors for dim stars. The second standard method – the weighted centre of mass method – is illustrated in Fig. 7. The presented results exhibit a better accuracy, but also large errors for dim stars. The best results – illustrated in Fig. 8 – are obtained with the proposed PSF-fitting method.

Determination of PSF at the beginning of image acquisition results in precise calculation of the stars' positions in the whole series of analysed images. The obtained results correspond to the reference data of all kinds of stars: S1, S2 and S3.

Table 1. The accuracy of centroid determination obtained with the standard and PSF-fitting methods.

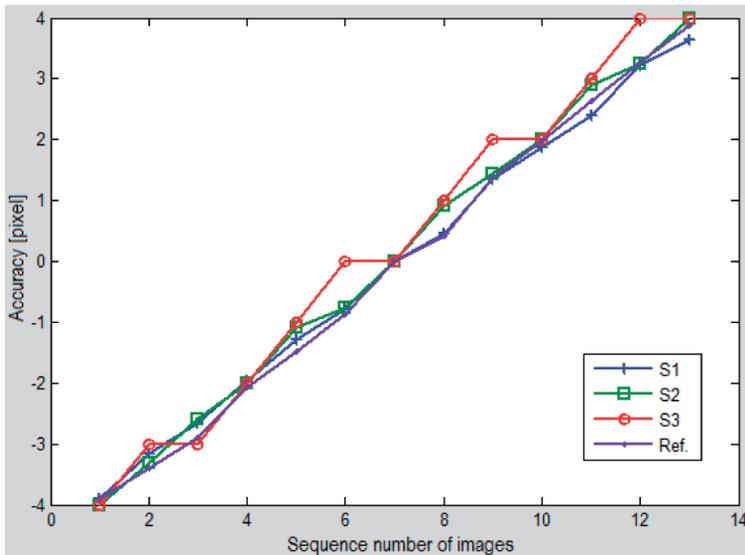| Img. No.	Centre of mass Δx [pixel]			Weighted centre of mass Δx [pixel]			PSF-fitting Δx [pixel]			Refer. Δx [pixel]
	S1	S2	S3	S1	S2	S3	S1	S2	S3	
1	−3.91	−4.00	−4.00	−3.52	−3.07	−0.77	−4.00	−4.00	−4.00	−3.91
2	−3.15	−3.31	−3.00	−3.01	−2.63	−0.75	−3.30	−3.30	−3.30	−3.39
3	−2.65	−2.60	−3.00	−2.43	−2.16	−0.71	−2.60	−2.80	−2.70	−2.91
4	−1.96	−2.00	−2.00	−1.85	−1.66	−0.62	−2.00	−2.10	−2.10	−2.08
5	−1.28	−1.09	−1.00	−1.25	−1.10	−0.44	−1.50	−1.30	−1.30	−1.49
6	−0.79	−0.76	0.00	−0.66	−0.59	−0.50	−0.60	−0.80	−0.60	−0.88
7	0.00	0.00	0.00	0.00	0.00	0.00	0.00	0.00	0.00	0.00
8	0.45	0.91	1.00	0.58	0.56	0.26	0.50	0.70	0.70	0.42
9	1.36	1.43	2.00	1.22	1.11	0.58	1.40	1.40	1.40	1.38
10	1.88	2.00	2.00	1.82	1.64	0.74	2.00	2.00	2.20	1.98
11	2.39	2.91	3.00	2.42	2.23	1.12	2.50	2.70	2.80	2.63
12	3.22	3.25	4.00	3.00	2.71	1.26	3.20	3.40	3.50	3.27
13	3.65	4.00	4.00	3.54	3.23	1.56	3.70	4.00	4.20	3.88

Fig. 6. The accuracy of centroid determination for the centre of mass method. The results for three different stars S1, S2, S3 and reference calculation.
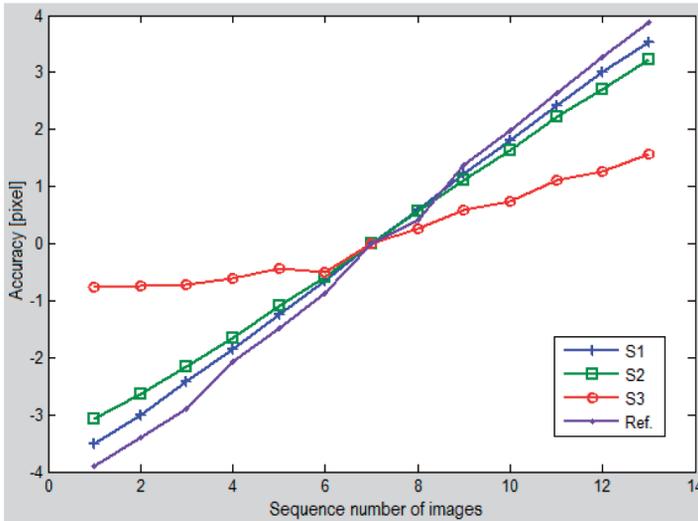
553

Fig. 7. The accuracy of centroid determination for the weighted centre of mass method. The results for three different stars S1, S2, S3 and reference calculation.
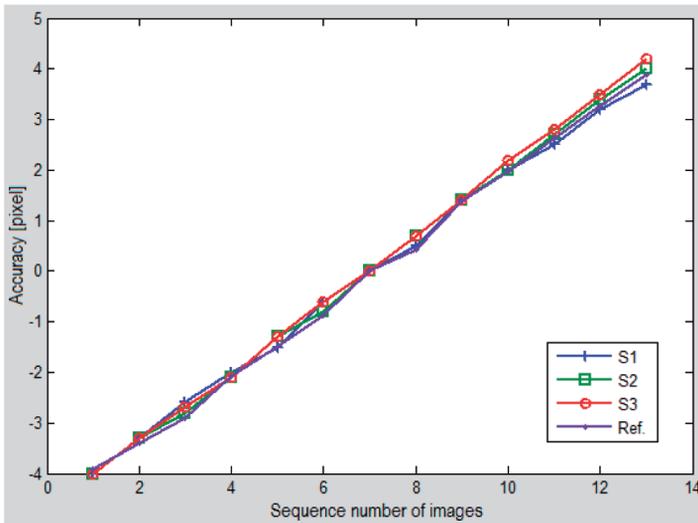

Fig. 8. The accuracy of centroid determination for the PSF-fitting method. The results for three different stars S1, S2, S3 and reference calculation.

For averaging the obtained results and in order to assess the quality of presented methods the root mean squared error (*RMSE*) was calculated. It can be expressed as follows:

$$RMSE = \sqrt{\frac{(\Delta x_{s1} - \Delta_{Ref})^2 + (\Delta x_{s2} - \Delta_{Ref})^2 + (\Delta x_{s3} - \Delta_{Ref})^2}{3}}, \qquad (2)$$

where: Δx_{s1}, Δx_{s2}, Δx_{s3},– the calculated position shifts of star centroid in coordinate *x* for stars S1, S2 and S3, respectively; Δx_{Ref} – the calculated image position shifts in coordinate *x* for the reference method.

Analysis of the results presented in Figs. 6, 7, 8 and 9 leads to the conclusion that the proposed PSF-fitting method of centroid calculation gives the best results. Two standard methods: the centre of mass and the weighted centre of mass methods give large deviations from the reference values, especially for the dark star S3. The calculated RMSE for the PSF-fitting method is several times smaller than that for the standard methods and this is true for all images in the series. The PSF-fitting could be used in calculation of stars' centroids in real deep sky images. This method is not time-consuming and is applicable in real-time ASIC or FPGA circuits [25–33].

Table 2. The root mean squared error of centroid determination with the standard and PSF-fitting methods.

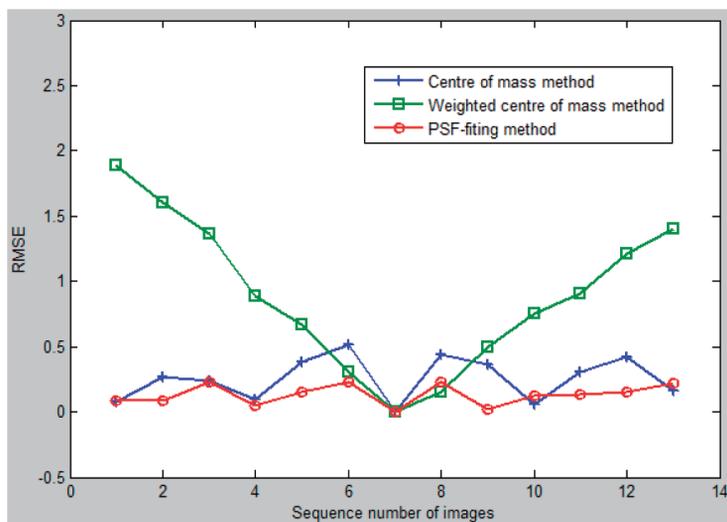| Img. No.	Centroid determination method		
	Centre of mass RMSE	Weighted centre of mass RMSE	PSF-fitting RMSE
1	0,0735	1,8887	0,0900
2	0,2690	1,5996	0,0900
3	0,2382	1,3669	0,2253
4	0,0950	0,8897	0,0490
5	0,3837	0,6635	0,1552
6	0,5151	0,3050	0,2332
7	0,0000	0,0000	0,0000
8	0,4384	0,1580	0,2332
9	0,3595	0,4946	0,0200
10	0,0594	0,7513	0,1281
11	0,3023	0,9103	0,1300
12	0,4224	1,2148	0,1578
13	0,1650	1,4043	0,2230

Fig. 9. The root mean squared error of centroid determination for three different methods: centre of mass, weighted centre of mass and PSF-fitting.

5. Conclusions

In this paper we proposed and analysed an algorithm for restoring astronomical images corrupted by turbulence effects and readout noise of a telescope system in order to determine the position of stars' centroid. A computation method has been used which employs an accurate centroid estimation algorithm using a reconstructed *point spread function* (PSF) from the recorded astronomical images.

A previously built tracking system described in other works [11–14] and our earlier works [1–5] uses the standard centre of mass method to calculate the reference star's position. It is a simple method that does not require large computations but does not take into account present atmospheric conditions and specific parameters of the optical system in a particular observation session. In this work we proposed a more complicated method of determining the reference star's position, using a reconstructed PSF. Since calculation of a specific PSF is performed before the start of an observation session, the required computational effort is not particularly significant. However, in the course of recording a series of long exposure images, during which the reference star's position is analysed cyclically, the already appointed PSF is used.

Limiting the calculations to a small section of the recorded image containing the guiding star enables reduction of the amount of needed calculations and implementation of a suitable real-time tracking system .

So far, the literature [15–18] has described PSF as useful for processing and enhancing the quality of already obtained images. The novelty of the solution described in this paper is using this method for analysing the images of the guiding star in real time, during acquisition of long exposure images of astronomical objects. The study carried out and discussed in this paper confirmed effectiveness of the proposed method and the possibility of its use in real-time systems.

The calculation experiment described in Section 4, performed on real astronomical images, showed an increased accuracy of determining the position of the reference star with the proposed method, in comparison with the standard methods. Simultaneously, computational complexity of the proposed method, assuming earlier determination of PSF, is not significantly higher than in the standard methods and enables its implementation in real-time tracking systems, described by us in the earlier literature [3–5].

Acknowledgements

References

[1] Suszyński, R., Wawryn, K., Dziebowski, M. (2015). An Efficient Algorithm for Determining Positions of Astronomical Objects in the Deep Sky Object Pictures. *Bulletin of the Polish Academy of Sciences-Technical Sciences*, 63(3), 679–684.

[2] Suszyński, R. (2009). Convolution Method for CCD Images Processing for DSO Astrophotography. *Proc. of the 52nd IEEE International Midwest Symposium on Circuits and Systems*,Cancun, Mexico, 762–765.

[3] Suszyński, R., Wawryn, K., Wirski, R. (2011). 2D image processing for auto-guiding system. *Proc. of the 54th IEEE International Midwest Symposium on Circuits and Systems*, Seoul, Korea, 1–4.

[4] Suszyński, R., Wawryn, K., Wirski, R. (2011). 2D signal processing for identification and tracking moving object. *Przeglad Elektrotechniczny*, 87(10), 126–129.

[5] Suszyński, R. (2008). Digital processing of CCD images for auto-guiding astrophotography system. *Proc. of the 15th International Conference on Mixed Design of Integrated Circuits and Systems*. Łódź, Poland, 559– 562.

[6] Suszyński, R., Wawryn, K. (Sep. 2014). An Improvement of Stars' Centroid Determination using PSF-fitting Method. *Proc. of the International Conference on Signals and Electronic Systems*, Poznań, Poland, 1–4.

[7] Hajek, M., Dezortova, M., Materka, A., Lerski, R. (2006). *Texture Analysis for Magnetic Resonance Imaging*. COST B21, Med4Publishing.

[8] Ogiela, M.R., Tadeusiewicz, R. (2008). Modern Computational Intelligence Methods for the Interpretation of Medical Images. *Studies in Computational Intelligence*, 84, Springer-Verlag.

[9] Mazur-Milecka, M., Nowakowski, A. (2011). Comparison of Tracking Methods in Respect of Automation of an Animal Behavioral Test. *Metrol. Meas. Syst.*, 18(1), 91–104.

[10] Pełczyński, P., Ostrowski, B., Rzeszotarski, D. (2012). Motion Vector Estimation of a Stereovision Camera with Inertial Sensors. *Metrol. Meas. Syst.*, 19(1), 141–150.

[11] McGuire, P.C., Sandler, D.G., Hart, M. L., Rhoadarmer, T.A. (1998). Adaptive optics: neural networks wavefront sensing, reconstruction, and prediction. J.W. Clark, T. Lindenau, M.L. Ristig (eds.). *Scientific applications of neural nets*, Springer-Verlag Publishers.

[12] Thomas, S., Fusco, T., Tokovinin, A., Nicolle, M., Michau, V., Rousset, G. (2006). Comparison of centroid computation algorithms in a Shack-Hartmann sensor. *Monthly Notices of the Rolay Astronomical Society*, 371, 323–336.

[13] Baker, K.L., Moalem, M.M. (2007). Iteratively weighted centroid of Shack-Hartmann wave-front sensors. *Opt. Express.*, 15, 5147–5159.

[14] Poyneer, L.A., Palmer, D.W., LaFortune, K.N., Bauman, B. (2005). Experimental results for correlation-based wave-front sensing. *SPIE*. 5894, 58940N.

[15] Vyas, A., Roopashree, M.B., Prasad, B.R. (2010). Cetroid detection by Gaussian pattern matching in adaptive optics. *International Journal of Computer Applications*, 1(26), 30–36.

[16] Noll, R.J. (1976). Zernike polynomials and atmosphere turbulences. *JOSA*, 66(3), 207–211.

[17] Berghi, A., Canedese, A., Masiero, A. (2007). Atmospheric turbulence prediction: a pca approach. *Proc. of the IEEE 46th Conference on Decision and Control*, 572–577.

[18] Jeffs, B.D., Christou, J.C. (1998). Blind bayesian restoration of adaptive optics telescope images using generalized gaussian markov random field models. *Proc. of the SPIE*, *Conference on Adaptive Optics and Telescope Systems*, 3353.

[19] Suszyński, R. (2009). Stand-alone station for deep space objects astrophotography. *Proc. of the 52nd IEEE Int. Midwest Symposium on Circuits and Systems*, Cancun, Mexico, 333–336.

[20] Zhang, W., Jiang, Z., Zhang, H., Luo, J. (2012). Optical Image Simulation System for Space Surveillance. *Proc. of the IEEE 26th Int. Parallel and Distributed Processing Symposium*.

[21] Li, C., Zhang, Y., Zheng, C., Hu, X. (2013). Implementing High-performance Intensity Model with Blur Effect on GPUs for Large-scale Star Image Simulation. *Proc. of Int. Conference on Image and Graphics*.

[22] Li, C.Z., Jin, S.Z. (2006). The Implement of High Speed Correlation Tracking Algorithm Based on FPGA in Space Solar Telescope. *Proc. of 8th International Conference on Signal Processing*.

[23] Zhai, C., Shao, M., Goullioud, R., Nemati, B. (2011). Micro-pixel accuracy centroid displacement estimation and detector calibration. *Instrumentation and Methods for Astrophysics*.

[24] Lee, S. (2002). Pointing accuracy improvement using model-based noise reduction method. *Proc. SPIE*, Mecherle, G.S. (eds.). *Free-Space Laser Communication Technologies XIV*, 4635, 65–71.

[25] Jendernalik, W., Blakiewicz, G., Handkiewicz, A., Melosik, M., (2013). Analogue CMOS ASICs in Image Processing Systems. *Metrol. Meas. Syst.*, 20(4), 613–622.

[26] Jendernalik, W., Jakusz, J., Blakiewicz, G., Szczepański, S., Piotrowski, R. (2012). Characteristics of an Image Sensor with Early-Vision Processing Fabricated in Standard 0.35 μm Cmos Technology. *Metrol. Meas. Syst.*, 19(2), 191–202.

[27] Jendernalik, W., Jakusz, J., Blakiewicz, G., Piotrowski, R., Szczepanski, S. (2011). CMOS realisation of analogue processor for early vision processing. *Bulletin of the Polish Academy of Sciences, Technical Sciences*, 59(2), 141–147.

[28] Blakiewicz, G. (2009). Analog multiplier for a low-power integrated image sensor. *Proc. of 16th Int. Conf. Mixed Design of Integrated Circuits & Systems MIXDES'09*, Łódź, Poland, 226–229.

[29] Handkiewicz, A., Lukowiak, M., Kropidlowski, M. (2002). Switched-current implementation of two-dimensional DCT for image processing. *15th Annual IEEE Int. Conf. on ASIC/SOC*, 186−190.

[30] Handkiewicz, A., Kropidlowski, M., Lukowiak, M., Bartkowiak, M. (2000). Switched-current filter design for image processing systems. *13th Annual IEEE International Conference on ASIC/SOC*, 8−12.

[31] Handkiewicz, A., Kropidlowski, M., Lukowiak, M. (1999). Switched-Current Technique for Video Compression and Quantization. *12th Annual IEEE International Conference on ASIC/SOC*, 299−303.

[32] Jendernalik, W., Blakiewicz, G., Jakusz, J., Szczepanski, S., Piotrowski, R. (2013). An Analog Sub-Miliwatt CMOS Image Sensor with Pixel-Level Convolution Processing. *IEEE Trans. Circuits Syst. I*, 60(2), 279−289.

[33] Jendernalik, W., Jakusz, J., Blakiewicz, G., *et al*. (2011). Analog CMOS processor for early vision processing with highly reduced power consumption. *20th European Conf. on Circuits Theory and Design (ECCTD)*, 745−748.